ACSNANO www.acsnano.org

ARTICLE

Effect of Chiral Ligand Concentration and Binding Mode on Chiroptical Activity of CdSe/CdS Quantum Dots

Vera A. Kuznetsova,[*,†,‡,▽] Eric Mates-Torres,[†,▽] Nadezda Prochukhan,[†] Madeline Marcastel,[†] Finn Purcell-Milton,[†,§] John O'Brien,[†] Anastasia K. Visheratina,[‡] Marina Martinez-Carmona,[†] Yulia Gromova,[†] Max Garcia-Melchor,[*,†] and Yurii K. Gun'ko[*,†,§]

[†]School of Chemistry, CRANN and AMBER Research Centres, Trinity College Dublin, College Green, Dublin 2, Ireland
[‡]ITMO University, St. Petersburg 197101, Russia
[§]BEACON, Bioeconomy SFI Research Centre, University College Dublin, Dublin 4, Ireland

Supporting Information

ABSTRACT: **Chiroptically active fluorescent semiconductor nanocrystals, quantum dots (QDs), are of high interest, from a theoretical and technological point of view, because they are promising candidates for a range of potential applications. Optical activity can be induced in QDs by capping them with chiral molecules, resulting in circular dichroism (CD) signals in the range of the QD ultraviolet−visible (UV-vis) absorption. However, the effects of the chiral ligand concentration and binding modes on the chiroptical properties of QDs are still poorly understood. In the present study, we report the strong influence of the concentration of a chiral amino acid (cysteine) on its binding modes upon the surface of CdSe/CdS QDs, resulting in varying QD chiroptical activity and corresponding CD signals. Importantly, we demonstrate that the increase of cysteine concentration is accompanied by the growth of the QD CD intensity, reaching a certain critical point, after which it starts to decrease. The intensity of the CD signal varies by almost an order of magnitude across this range. Nuclear magnetic resonance and Fourier transform infrared data, supported by density functional theory calculations, reveal a change in the binding mode of cysteine molecules from tridentate to bidentate when going from low to high concentrations, which results in a change in the CD intensity. Hence, we conclude that the chiroptical properties of QDs are dependent on the concentration and binding modes of the capping chiral ligands. These findings are very important for understanding chiroptical phenomena at the nanoscale and for the design of advanced optically active nanomaterials.**

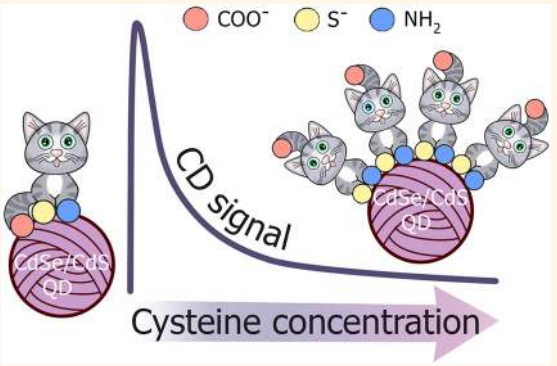

KEYWORDS: *chirality, quantum dots, chiroptical activity, cysteine, ligand concentration, binding mode, density functional theory*

Chirality is among the most fascinating occurrences in the natural world. A chiral molecule is one that has two mirror-image forms, i.e., enantiomers, which are nonsuperimposable in three dimensions. Well-known examples of chiral molecules are proteins, DNA, sugars, amino acids, enzymes, and drugs such as ibuprofen and L-Dopa, which is a drug for the treatment of Parkinson's disease. Overall, chirality is one of the most important factors in biomolecular recognition, and, therefore, chiral compounds play a very significant role in chemistry, biology, pharmacy and medicine. Chirality has also been envisaged to play an important role in nanotechnology, and recently, the area of chiral nanomaterials has received a great deal of attention, because of the range of potential applications offered by these materials. Chiroptically active quantum dots (QDs)—fluorescent semiconductor nanocrystals with tunable optical properties—have also been intensively studied in the last two decades[1,2] since they were first reported in 2007.[3] Chiral QDs have several potential applications,[1,2,4−7] such as biological sensors,[8−17] anticounterfeiting material,[18,19] as well as components in photonic[20−23] and in spin-polarized devices.[24−26]

Optical activity can be induced in QDs by functionalization with chiral ligands via a relatively simple post-synthetic phase-transfer ligand exchange.[1,4,27−40] In this process, the initial hydrophobic ligands in QDs produced by the hot injection

Received: September 23, 2019
Accepted: November 7, 2019
Published: November 7, 2019

DOI: 10.1021/acsnano.9b07513
ACS Nano XXXX, XXX, XXX−XXX

synthesis in organic medium are typically exchanged by chiral hydrophilic ligands, accompanied by the transfer of QDs into the aqueous phase.[16,33,35,37] In this case, QDs exhibit optical activity in their absorption region, unlike the chiral ligand molecules, which typically absorb light only in the deep UV region.[33,37] The origin of induced chirality can be explained by the chiral distortion of QD surface atoms upon the adsorption of chiral ligands,[3,34,41,42] or the hybridization of the energy levels of the QD and chiral ligand molecules leading to the splitting of QD hole−electron levels into two sublevels with different absorptions of circularly polarized light.[33,38,40,43−47]

The phenomenon of induced chiroptical activity in nanoparticles has attracted considerable attention, and, currently, it is being intensively studied. The shape of QD circular dichroism (CD) spectra and the magnitude of induced CD bands are dependent on many factors, including the nature of the material and the size of the QD core,[29,40] QD shape and anisotropy,[1,31,35−37,48−50] the nature and thickness of the QD shell,[33,34,40] and the chemical composition and coordination modes of the ligands.[27,28,32,51] The concentration of chiral ligands used during the QD synthesis has also been reported to influence the intensity of CD signal of nanoparticles,[31,52] but the addition of different amounts of ligands to the synthetic medium leads to the formation of nanoparticles with different morphology, which is proven to be the main reason for the changes observed in the CD spectra. Hence, the effect of the chiral ligand concentration is still unclear, and it is yet to be demonstrated.

Herein we report a detailed investigation of the effect of chiral L-cysteine ligands (hereafter referred simply as Cys) concentration and binding mode on the CD intensity of the CdSe/CdS QDs, which were prepared by an exchange of achiral organic ligands with chiral Cys ligands. We have found that the dependence of QD CD signal intensity on Cys concentration is nonlinear; initially, the CD signal peak intensity increases with Cys concentration, followed by a decrease when a further excess of ligands is added. Moreover, CD intensity changes dramatically, depending on ligand concentration, by up to 1 order of magnitude, which makes it one of the key factors that should be taken into account during the investigation of chiroptical properties of nanoparticles. By using NMR and FTIR spectroscopy and density functional theory (DFT) calculations, we have shown that, while at low concentrations, Cys ligands are bound to the QD surface in a tridentate coordination, an increase of the Cys concentration switches the coordination trend toward bidentate binding modes. Furthermore, our DFT approach has allowed us to assess the stabilization of the Cys ligands quantitatively via noncovalent interactions at different ligand concentrations and to clearly pinpoint these interactions. We believe these studies are of great theoretical and practical importance, because they provide a fundamental understanding of chiroptical phenomena at the nanoscale, by considering chiral ligand concentrations, ligand−ligand interactions, and their binding modes at the QD surface. Hence, this research is envisioned to contribute to the design of advanced chiroptically active nanomaterials by leveraging an optimal ligand concentration to maximize the CD response and improve signal-to-noise ratio for potential applications such as CD spectroscopy, optical sensing, metamaterials, and nanophotonics.

RESULTS AND DISCUSSION

Effect of Cys Concentration on the Chiroptical Activity of CdSe/CdS Core/Shell QDs. CdSe/CdS QDs (hereafter referred as QDs) were synthesized via the well-documented SILAR hot injection technique.[33,53] QDs were characterized by UV-Vis, PL, and CD spectroscopy and transmission electron microscopy. The diameter of the QDs obtained was 5.2 ± 0.8 nm, while the thickness of the CdS shell was 1.2 ± 0.4 nm, which corresponds to five monolayers of CdS. Full characterization of QDs can be found in the Supporting Information. Original hydrophobic ligands (mostly oleylamine) of QDs were subsequently displaced by L- and D-cysteine, using a previously reported phase-transfer procedure.[14] Briefly, a Cys solution in methanol was added to the QD chloroform solution, then shaken, and left for 2 min to allow Cys to replace the hydrophobic ligands. After that, an aqueous 0.01 M KOH solution was added and the Cys-functionalized QDs were transferred to the aqueous phase. As a result, the QDs became water-soluble and chiroptically active, which is reflected in the appearance of mirror-imaged CD signals in the region of QD absorbance including the excitonic area (Figure 1). CD signal corresponding to the QD

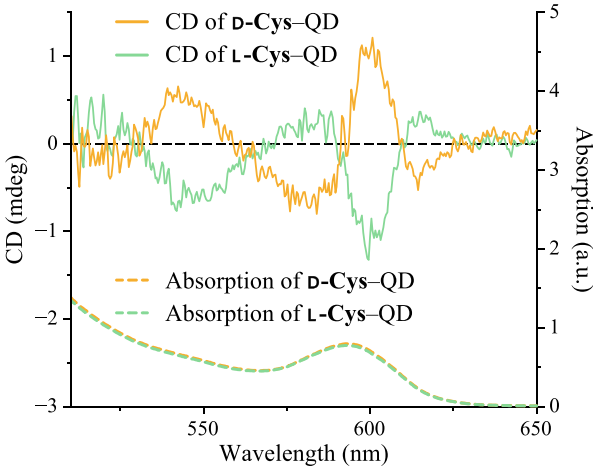

Figure 1. CD spectra (solid lines) and UV-vis spectra (dotted lines) of D-Cys-functionalized CdSe/CdS QDs (orange) and L-Cys-functionalized CdSe/CdS QDs (green). Cysteine concentration = 0.42 mg/mL.

exciton is produced due to the hybridization of the degenerated valence band energy level of QDs and HOMO level of Cys molecules yielding two sublevels. The resulting optical transitions from these sublevels have a contra-directional rotary strength, which is reflected in the splitting of CD signal for positive and negative bands crossing zero in the vicinity of exciton maximum.[27−29,33,34,40,49]

To study the influence of Cys concentration on QD chiroptical response intensity, a ligand exchange was performed using different amounts of Cys, varying from 0.1 mg/mL to 1.6 mg/mL. We note that it was not technically possible to perform the procedure with higher amounts of Cys ligand, because of the limited solubility of Cys in methanol. Thus, extra amounts (3 and 10 mg/mL) were added to the aqueous solutions of Cys QDs to achieve the even-higher Cys concentration of 4.6 and 11.6 mg/mL. *G*-factor curves of Cys-functionalized QDs after phase transfer with different amounts of Cys are illustrated in Figure 2a. The *G*-factor was used

DOI: 10.1021/acsnano.9b07513
ACS Nano XXXX, XXX, XXX−XXX

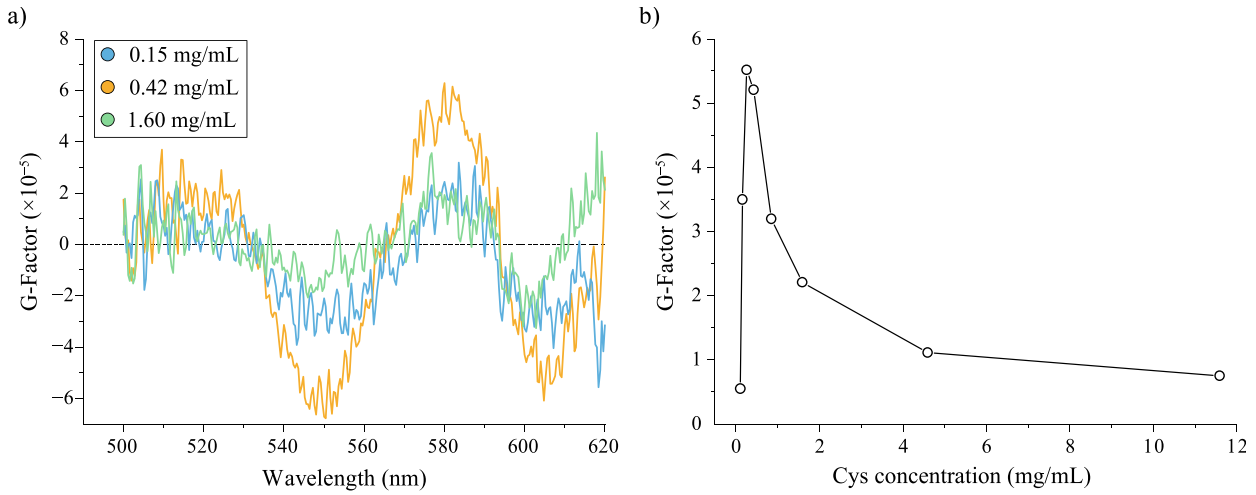

Figure 2. (a) *G*-factor graphs of Cys-functionalized CdSe/CdS QDs with varying Cys concentrations: 0.15, 0.42, and 1.60 mg/mL. (b) Dependence of the *G*-factor intensity in the excitonic region of Cys CdSe/CdS QDs at 605 nm on Cys concentration.

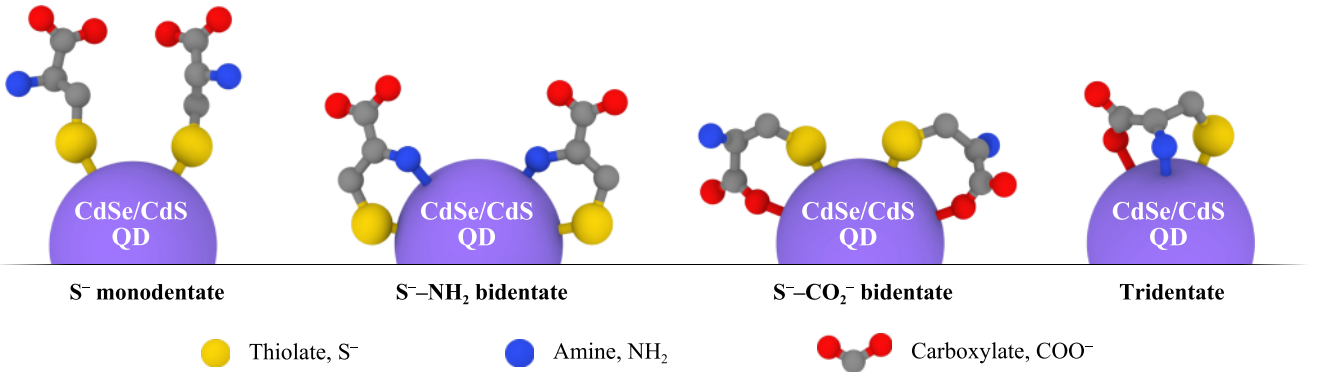

Figure 3. Possible binding modes of Cys ligand on the QD surface (from left to right): S^- monodentate, S^-–NH_2 bidentate, S^-–CO_2^- bidentate, and tridentate.

instead of CD signal to avoid the effect of the QD concentration influence. The *G*-factor is defined as $G = \Delta\varepsilon/\varepsilon = (A_L - A_R)/A$, where A_L and A_R are the absorbance of left-handed and right-handed circularly polarized light, respectively, and A is the absorbance of unpolarized light. It was found that the *G*-factor intensity varied with the Cys concentration in a nonlinear fashion. Similar results were also obtained for D-Cys QDs (see Figure S3 in the Supporting Information). The dependence of the *G*-factor intensity of the maximum peak corresponding to the QD excitonic region on Cys concentration is shown in Figure 2b. The *G*-factor intensity increased initially with Cys concentration. However, after a critical Cys concentration (i.e., 0.26 mg/mL) was achieved, the QD *G*-factor intensity reached a maximum and started to decrease. In light of these striking observations, we decided to perform more-detailed investigations.

Determination of Cys Binding Mode on the QD Surface. One explanation for the reduction of the *G*-factor might be the change of the Cys binding mode with the Cd^{2+} ions on the QD surface upon increasing the amount of Cys ligands in solution. Indeed, it was previously reported that the shape of the QD CD spectra is strongly dependent on the coordination mode of chiral ligands on the QD surface,[27,28,32,54,55] but the dependence of the intensity of the QD CD signals and the coordination of the ligands on their concentration has not been explored to date.

The Cys ligand at the experimental pH of 13 has three moieties: thiolate (S^-), carboxylate (COO^-), and amino (NH_2) functional groups. Potentially, all of them can be coordinated to Cd^{2+} ions on the QD surface, although S^- has the strongest affinity to Cd^{2+} ions. Thus, cysteine can bind to the QD surface via all three groups (tridentate), via a combination of S^- and NH_2 (S^-–NH_2 bidentate) or S^- and COO^- (S^-–COO^- bidentate), and solely via the S^- (monodentate). All of these possible Cys binding modes are depicted in Figure 3.

Some investigations of Cys binding modes on the surface of Cd-based clusters and nanoparticles have been previously reported. For example, by performing multinuclear (^1H, ^{13}C, ^{77}Se, ^{15}N, ^{113}Cd, and ^{23}Na) solid-state NMR techniques, Takegoshi et al. have shown that Cys ligand binds with $CdSe_{34}$ magic clusters via coordination to Cd^{2+} ions as S^-–NH_2 bidentate and S^- monodentate ligand, in amounts of 43% and 57%, respectively.[56−58] In another study using ^{13}C solid-state NMR,[29] it was demonstrated that Cys binds to the surface of 2.9 nm CdSe QDs as a S^-–COO^- bidentate ligand. Density functional theory (DFT) calculations[59] revealed that the interaction patterns between Cys and $(CdSe)_n$ vary with the cluster size and medium. Pattern S → Cd ← N is preferred in the gas phase, toluene, and alkaline solution, while pattern O → Cd and H → Se is preferred in water. In another study,[60] DFT calculations were performed on complexes of $(CdSe)_{13}$

DOI: 10.1021/acsnano.9b07513
ACS Nano XXXX, XXX, XXX−XXX

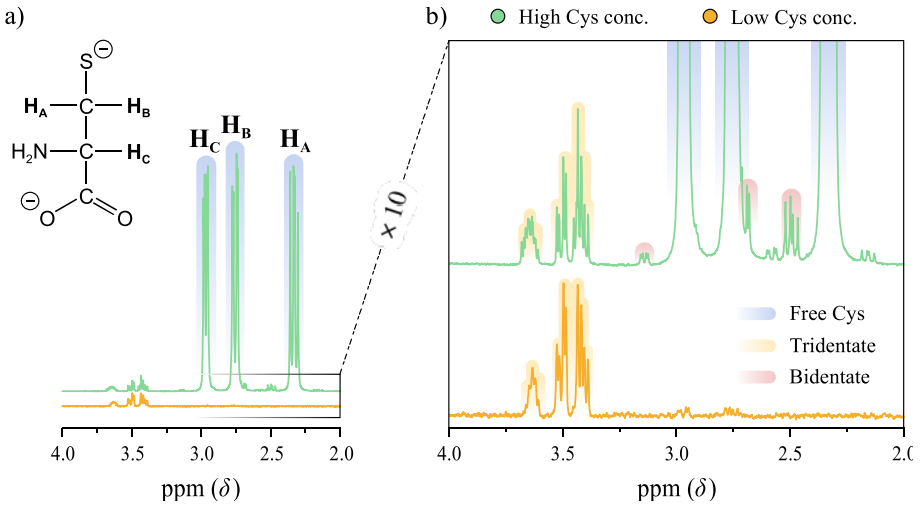

Figure 4. (a) ^{1}H NMR spectra of QDs in H_2O with high and low Cys concentration at pH 13 for free Cys, and (b) scaled-up ^{1}H NMR spectra of QDs with high and low Cys concentrations, including peaks of bound Cys.

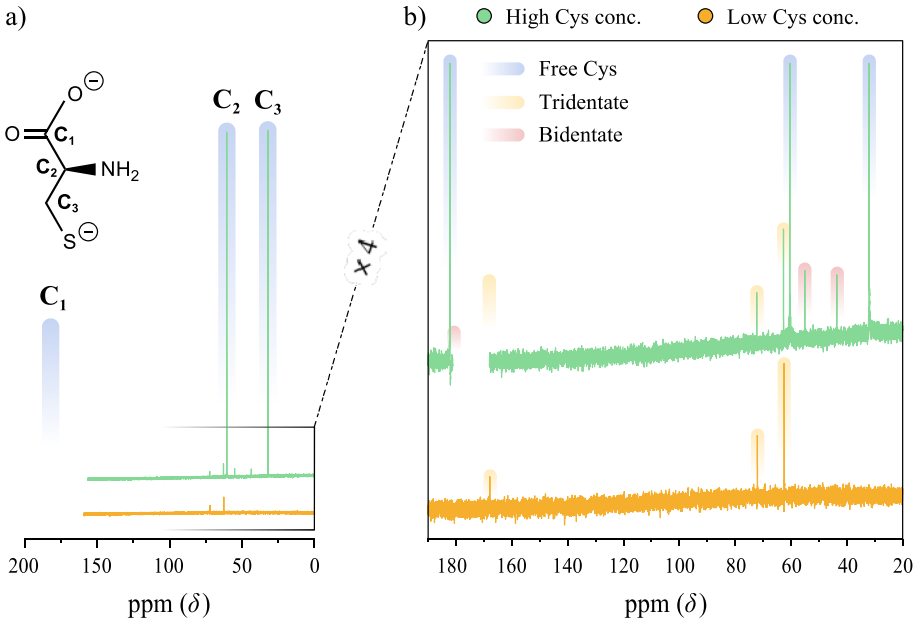

Figure 5. (a) ^{13}C NMR spectra of QDs aqueous solutions with high and low Cys concentration at pH 13 for free Cys, and (b) scaled-up ^{13}C NMR spectra of QDs with high and low Cys concentrations, including peaks of bound cysteine.

nanoclusters and Cys molecules attached as tridentate ligands to the distorted surface of the nanoclusters. Hence, it is known that binding modes of Cys are dependent on many factors such as medium, pH, cluster size, etc.

Previous studies on aqueous metal complexes have demonstrated that the Cys binding mode is also dependent on the ratio between the Cys and metal ions. For example, Cys can be coordinated to Pb^{2+} ions in a tridentate fashion in 1:1 complexes, while in 2:1 complexes, it binds in a bidentate fashion.[61] Prompted by these results, we suggested that the concentration of Cys might influence its binding mode, and, consequently, the *G*-factor intensity of Cys-stabilized QDs.

Investigation of Cys Binding Modes by NMR Spectroscopy. To investigate how the Cys concentration influences its binding mode on the QD surface, ^{1}H and ^{13}C NMR spectroscopy analyses of two different Cys QD solutions were performed: (1) a solution with a "low" Cys concentration (ca. 0.2 mg/mL), at which *G*-factor increased, and (2) a solution with a "high" Cys concentration (ca. 20 mg/mL), corresponding to the region where the *G*-factor is minimum. Cys-QD solutions for NMR analysis were prepared and measured under argon atmosphere to avoid Cys oxidation.

^{1}H NMR Spectroscopy. The ^{1}H NMR spectrum of free Cys at pH 13 is different from one at neutral pH.[61] It has the form of three double doublets (Figure 4a), corresponding to a H atom bound to a C_2 atom with a chemical shift of 2.97 ppm (^1H_C), and two H atoms bound to C_3, which are chemically inequivalent, with 2.33 and 2.75 ppm chemical shifts (^1H_A and ^1H_B, respectively). The carboxylic and thiol groups are deprotonated at pH 13 (pK_a = 1.71 for −COOH and pK_a = 8.27 for −SH),[62] and accordingly, the ^{1}H NMR spectra did not display any signals arising from protons on these groups. We note that the ^{1}H NMR peak of the amino group is not usually observed in aqueous solutions.[63,64]

DOI: 10.1021/acsnano.9b07513
ACS Nano XXXX, XXX, XXX−XXX

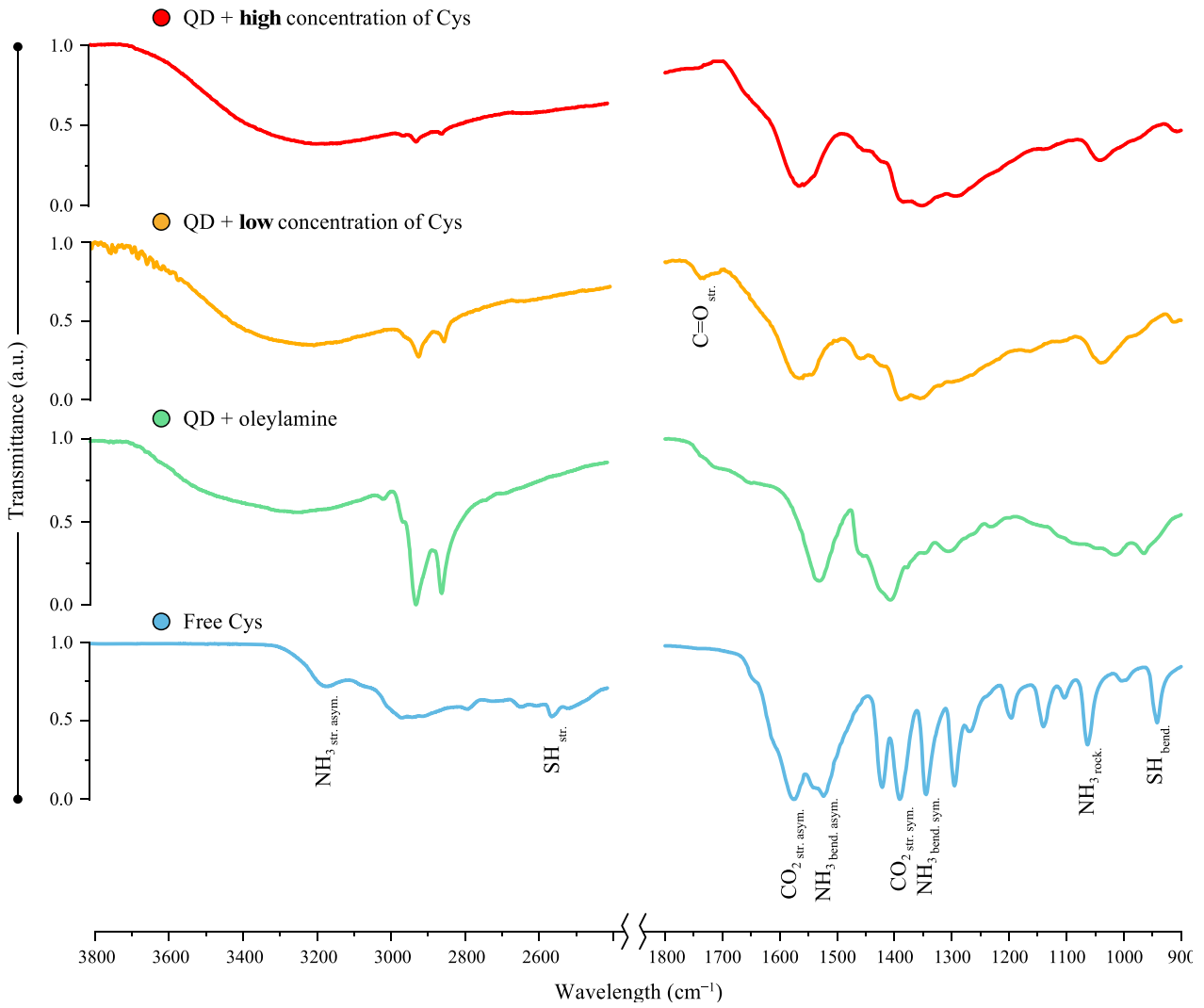

Figure 6. FTIR spectra of QDs precipitated from aqueous solutions with a high and low Cys concentration, QDs with organic ligands—mostly oleylamine and free cysteine. Full FTIR spectra are presented in Figure S4 in the Supporting Information.

At a low Cys concentration, almost all ligands are bound to the QD surface, and only one set of peaks corresponding to the tridentate[61] binding mode of the molecules is observed in the ^{1}H NMR spectrum. This can be seen in Figure 4b (orange line), where peaks were shifted downfield, compared to free Cys ($^{1}H_A$, $^{1}H_B$, and $^{1}H_C$ shifted from 2.33, 2.75, and 2.97 ppm to 3.42, 3.50 and 3.63 ppm, respectively).[61] At a high Cys concentration, three sets of ^{1}H NMR peaks were observed (Figure 4b, green line): (i) the first intense peak set corresponds to the free Cys; (ii) the second one presents the same peaks associated with the tridentate mode registered in the spectrum at low Cys concentration; and (iii) the third one corresponds to the bidentate form. In the case of the bidentate mode, the $^{1}H_B$ peak is shifted downfield, with respect to the free Cys form, which corresponds to the S^- binding to Cd^{2+}, while the $^{1}H_C$ peak did not shift very much, compared to the tridentate form, indicating that the COO^- is most likely free.

^{13}C NMR Spectroscopy. ^{13}C NMR results were consistent with the ^{1}H NMR data. Each Cys molecule has three carbon atoms, with the following ^{13}C NMR peaks: $^{13}C_1$, representing the C atom of the carboxylic group; $^{13}C_2$ and $^{13}C_3$, representing the C atoms bound to NH_2 and S^- groups with the peak positions at 179, 59, and 29 ppm, respectively (Figure 5a). At low concentrations (Figure 5b, orange lines), only one set of Cys peaks (different from that of the free molecule) can be observed, indicating that almost all cysteine molecules are bound to the QD surface. Besides, all three signals present a significant shift in position (from 179 ppm to 168 ppm for the carboxylic $^{13}C_1$,[65] from 59 ppm to 72 ppm and from 29 ppm to 62 ppm for the aminated $^{13}C_2$ and the thiolated $^{13}C_3$, respectively),[66] suggesting that, at low concentrations, Cys is coordinated in a tridentate mode.

At the higher Cys concentration (Figure 5b, green lines), the ^{13}C NMR spectrum presents three sets of peaks: (i) the first one, with three intense signals at the same positions as free Cys; (ii) the second one, with three weak peaks corresponding to the low concentration ones; and (iii) the third one, where $^{13}C_1$ remains almost in the same position, but $^{13}C_2$ and $^{13}C_3$ are shifted from 59 ppm to 55 ppm and from 29 ppm to 44 ppm, respectively. Similar shifts have been reported for a NH_2−SH bidentate mode;[67] therefore, we attribute these signals to Cys molecules that are bound to the QD surface in a S^-−NH_2 bidentate configuration.[67]

Investigation of Cys Binding Modes by FTIR Spectroscopy. To determine the binding mode of the amino

DOI: 10.1021/acsnano.9b07513
ACS Nano XXXX, XXX, XXX−XXX

group, which was not obvious from NMR analysis, we have also performed FTIR analysis of our QD samples. To prepare the samples for our FTIR studies, Cys-stabilized QDs were precipitated from aqueous solutions with high and low Cys concentrations, using acetone, and subsequently dried. It is important to note that samples did not contain water, which has a very broad and intense peak in the 3000−3750 cm^{-1} region that overlaps with the asymmetrical stretching vibration peaks of the amino group. Cys-QDs spectra are provided in Figure 6 for comparison with QDs functionalized with initial organic ligands (mostly oleylamine) and with pure Cys.

The S^- group of free Cys has two peaks at 2550 and 942 cm^{-1}, corresponding to its stretching and bending modes, respectively. Both peaks are absent in the spectra of Cys-QDs. The NH_2 group of free Cys has a peak associated with asymmetrical stretching vibrations at 3165 cm^{-1}, which is significantly broadened when NH_2 is bound to the QD surface. This broadening can be observed in the spectra of QDs with oleylamine and QDs with Cys, both at high and low concentrations, confirming that the amino group is coordinated with the QD surface. Pure Cys has a zwitterionic form with a deprotonated carboxylic group (COO^-) and a protonated amino group (NH_3^+). The free negatively charged carboxylic group has asymmetric and symmetric stretching vibration peaks at 1575 and 1391 cm^{-1}, respectively. The appearance of a carbonyl stretching mode peak at 1735 cm^{-1} on the FTIR spectra of QDs with a low Cys concentration indicates the binding of the COO^- group. QDs with a high amount of Cys ligands display a smaller peak at this area, indicating that part of the COO^- groups are free. This is in full agreement with the NMR data.

Effect of Cys Binding Mode on the Ligand Configuration on the QD Surface. The Cys molecule has three staggered rotamers as the result of rotation along the C_2-C_3 axis (*a*), namely, a *trans*-rotamer, where the carboxyl and thiol groups are in *trans* position, and two *gauche*-rotamers, where these groups are separated by a torsion angle of 60° (see Figure 7a).

Previous reports of NMR studies of Pb^{II}-based Cys complexes have shown that, under alkaline conditions, when COOH and SH groups of free Cys are deprotonated and negatively charged, the *trans* rotamer is prevalent.[61] Therein, it was also demonstrated that if the Cys ligand is bound to Pb metal ion through all three functional groups, NMR spectra mostly correspond to the *gauche-h* rotamer, i.e., all three groups are located at one side of the molecule, which facilitates tridentate Cys binding. When Cys is coordinated via a S^-−NH_2 bidentate mode, both conformations are present in solution, but the *trans* rotamer is prevalent. However, in our system, when Cys is bound to the QD surface, the *trans* rotamer can be even more preferable, because of steric constraints.

Other previous studies have shown that one type of enantiomer of a chiral molecule can bind to the nanoparticle surface in different ways.[28,55] For example, acetyl-L-Cys can bind to HgS via the SH and COOH groups or SH and Ac groups, depending on the synthesis conditions.[55] Sometimes, these bound molecules exhibit almost mirror-image configurations on the QD surface, which gives rise to inverted CD spectra. These results were further confirmed by theoretical calculations.[28]

In our study, Cys can bind to the QD surface in a tridentate and S^-−NH_2 bidentate fashion, as was shown above, based on FTIR and NMR data, and Cys molecules in these two coordination modes can adopt different rotamers: the *gauche-h* rotamer for the tridentate binding mode, and, prevalently, the *trans* rotamer for the bidentate coordination (see Figure 7b). These two rotamer forms bound to the QD can be considered as almost diastereomers of each other, with respect to the relative position of the S^- and the NH_2 groups. Hence, we suggest that, because of these diastereomeric conformations, Cys bound in bidentate and tridentate modes can be the origin of the opposite CD signals. Therefore, at high concentrations, when the amount of Cys molecules bound in a bidentate mode increases, the CD signal produced by the tridentate ligands at low concentrations is partially compensated, resulting in an overall decrease of the CD signal.

Computational Studies of Cys Binding Modes. Based on the experimental observations presented above, a likely explanation for the change in the coordination of the adsorbed Cys ligands upon increase of Cys concentration is the emergence of ligand−ligand interactions. To confirm this, we conducted a thorough investigation by means of periodic DFT calculations (see the Materials and Methods section for details) in order to elucidate the binding modes of Cys molecules on the QD surface at different concentrations. Following an exhaustive iterative coverage analysis, we selected five theoretical models featuring 1−5 Cys molecules adsorbed on a $p(3 \times 3)$ supercell of a CdS(0001) surface—corresponding to the structure of the exposed QD shell—with the objective of reproducing low, intermediate, and high coverage limits, respectively. For each surface coverage, we then considered all possible combinations of binding modes, rendering a total of 67 different structures. The results obtained for the most energetically favorable adsorptions are summarized in Figure 8, which also displays the binding modes adopted by each of the ligands per unit cell.

The analysis of the most stable configurations of the low-coverage model (Figure 8a) revealed that Cys ligands are predominantly bound to the QD surface in a tridentate conformation with the S^-, COO^-, and NH_2 groups coordinated to surface Cd^{2+} ions, in agreement with experiments. As can be seen in Figure 8b, the addition of a second ligand did not affect the Cys binding mode in the lowest

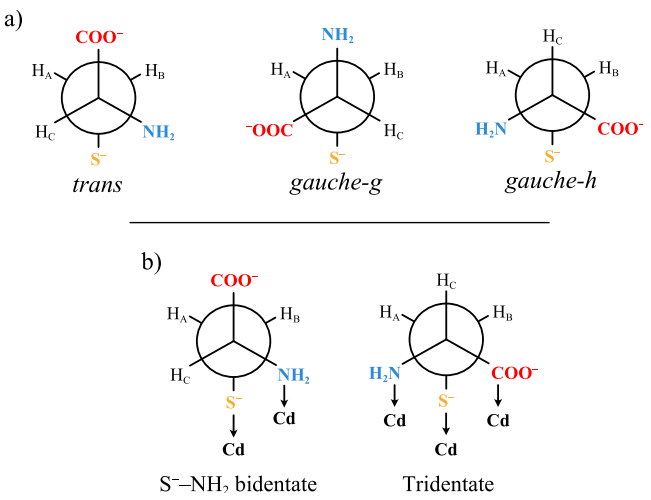

Figure 7. (a) Newman projections of the three rotamers of the Cys molecule. (b) Newman projections of S^-−NH_2 bidentate (left) and tridentate (right) coordination modes of Cys on the QD surface.

DOI: 10.1021/acsnano.9b07513
ACS Nano XXXX, XXX, XXX−XXX

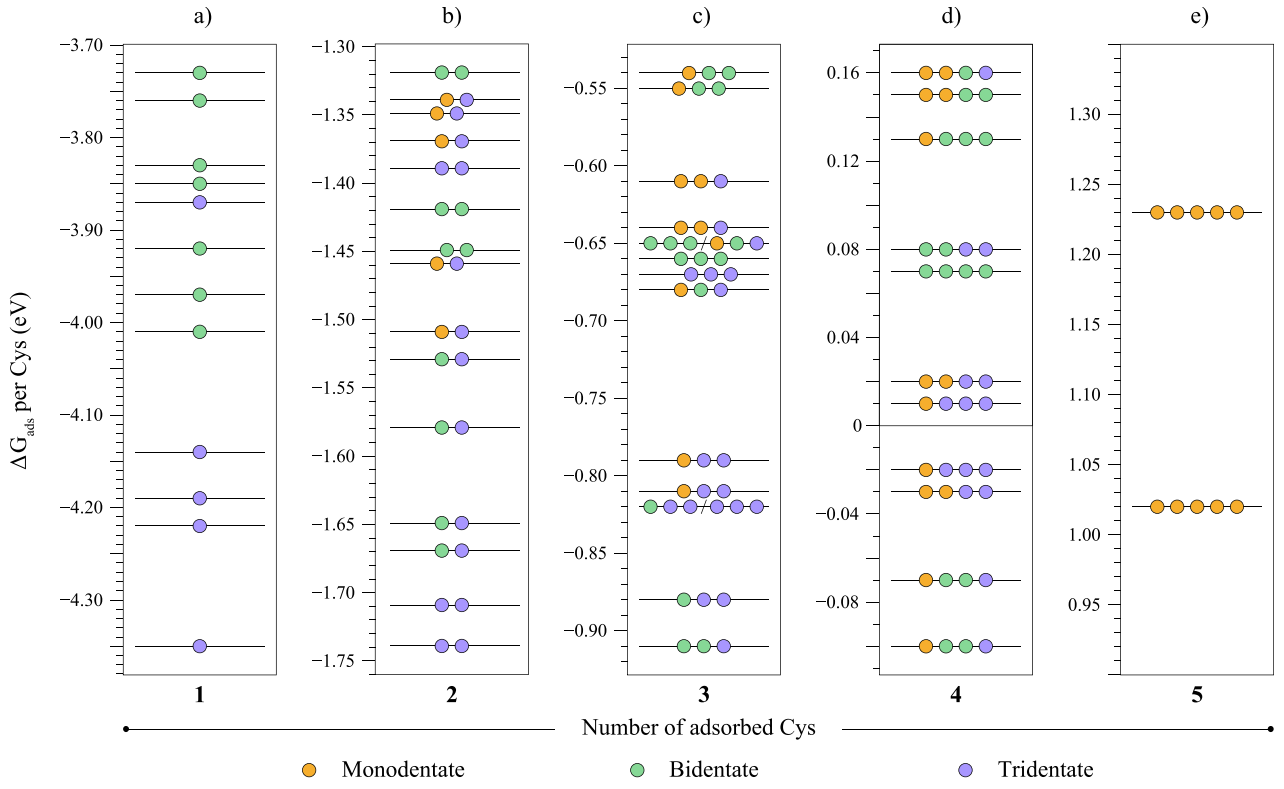

Figure 8. Calculated adsorption Gibbs energies, ΔG_{ads}, for the (a) low, (b, c) intermediate, and (d, e) high coverage models with 1−5 Cys molecules per unit cell. Each line represents a different configuration of the ligands within a given coverage. Monodentate, bidentate, and tridentate Cys binding modes are represented as orange, green, and purple circles, respectively. Gray areas indicate endergonic configurations; therefore, these are predicted to be unlikely. We note that, in panel (c), there are two sets of configurations that possess the same ΔG_{ads} value, up to the second decimal digit; these are represented on the same line and separated by a slash.

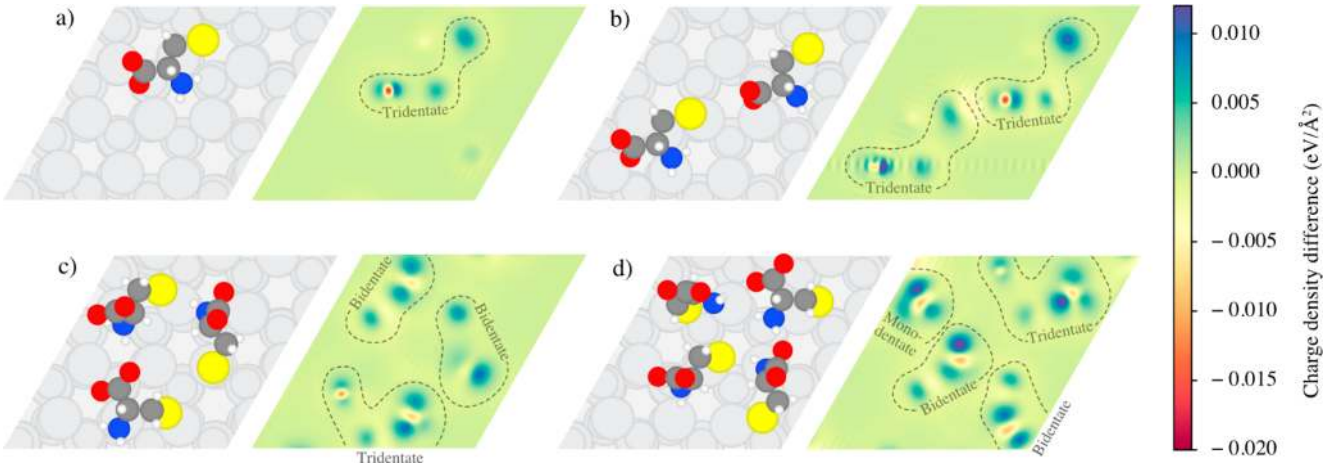

Figure 9. Optimized structures of the most stable configurations with a predicted exergonic adsorption for the (a) low, (b, c) intermediate, and (d) high coverage models featuring 1−4 Cys, alongside a 2D plot of the charge density difference across the interaction plane. [Atom color code: C (gray), H (white), N (blue), O (red), and S (yellow).]

energy configuration. However, DFT calculations predict the emergence of a relatively stable configuration (only 70 meV higher in energy, with respect to the lowest energy configuration) in which one of the Cys ligands becomes bidentate through the S^- and NH_2 groups, while the other one remained coordinated in a tridentate mode. This original configuration points toward a decrease in the prevalence of the tridentate mode at higher Cys coverages, which, again, is consistent with experimental observations. This was indeed observed upon the addition of the third and fourth Cys ligands in the intermediate and high coverage models depicted in Figures 8c and 8d. In both cases, the bidentate conformation was found to predominate in the most stable configurations, where even a monodentate Cys was predicted to coexist on the surface covered with four ligands. An inclusion of a fifth Cys molecule was revealed to be energetically unfeasible based on the endergonic ΔG_{ads} values obtained for the models depicted in Figure 8e. The differential adsorption of the Cys in each coverage model is depicted in Figure S5 in the Supporting Information.

DOI: 10.1021/acsnano.9b07513
ACS Nano XXXX, XXX, XXX−XXX

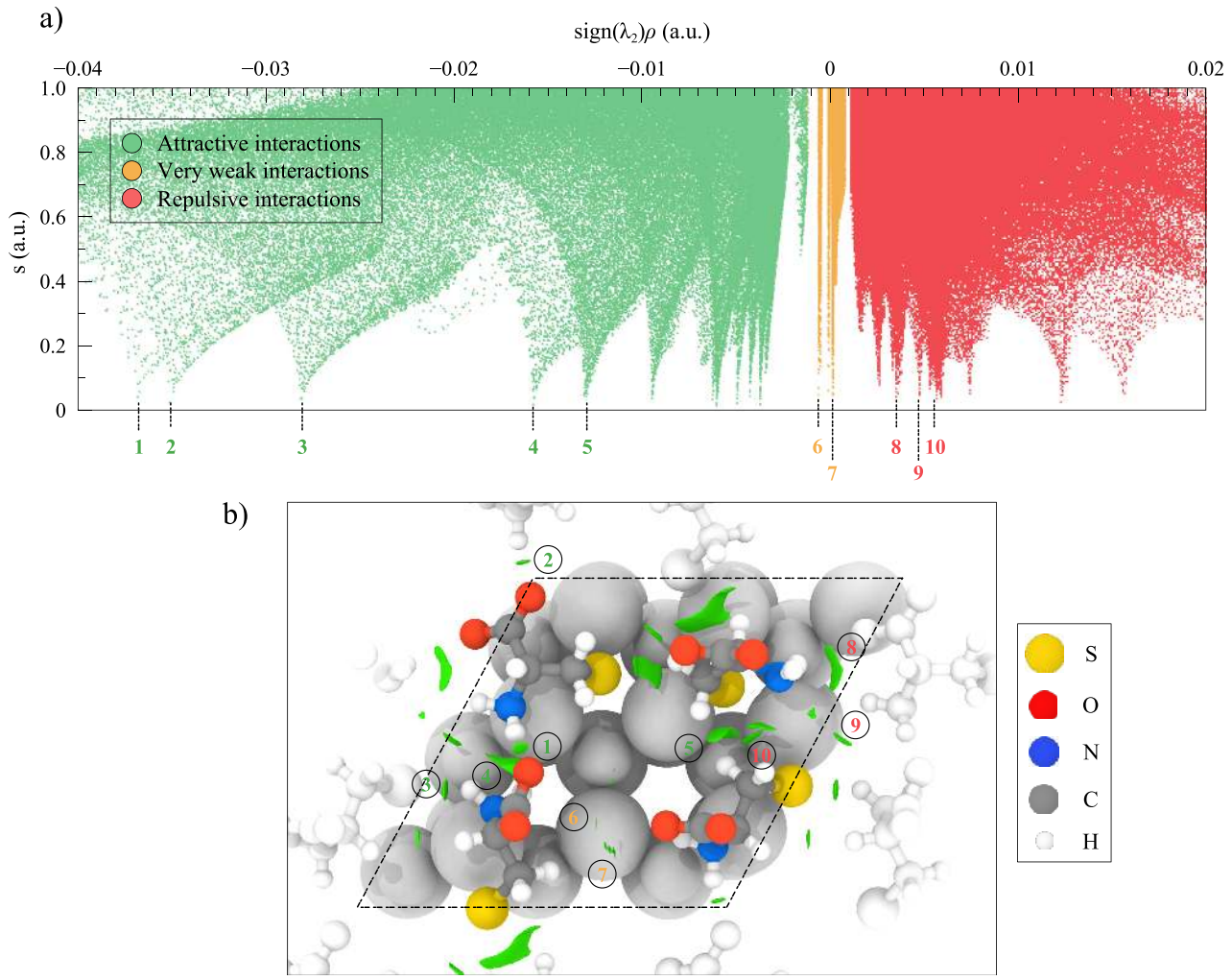

Figure 10. (a) Plot of *s*, as a function of sign(λ_2)ρ. (b) Representation of the intermolecular noncovalent interactions inside a unit cell, displayed as a green isosurface with an isovalue of 0.45 $e^-/(a.u.)^3$. The 10 most relevant interactions are labeled in both the reduced density gradient plot and the representation of the noncovalent interactions. Atoms of Cys ligands from neighboring unit cells are colored white, while Cd and S atoms from the QD surface are colored light gray for clarity.

The lowest energy structures from the coverages including 1−4 Cys ligands are represented in Figure 9, alongside two-dimensional (2D) plots of the charge density differences between the ligands and the QD surface. In these plots, warmer (orange and red) and colder (turquoise and blue) colors indicate a decrease and increase, respectively, in the charge density difference across the interaction plane. Hence, functional groups that lay on higher or lower charge-density difference regions are predicted to interact with the QD surface. This allows one to confirm the binding mode of each adsorbed Cys molecule, based on the number of functional groups laying on these regions.

To understand the change in the Cys binding mode observed from tridentate to bidentate and monodentate at high ligand concentrations, we subsequently analyzed the intermolecular noncovalent interactions (NCIs) on QD surfaces terminated with 2−5 Cys molecules (see the Materials and Methods section for details)—the low coverage model with 1 Cys per unit cell was not considered, since ligands in periodic images are too far apart to interact noncovalently. Importantly, the methodology employed herein allows for the semiquantitative analysis of these interactions by identifying the regions in which the atomic clouds of the Cys molecules overlap. In short, since the electron density in these regions is maximum, the reduced density gradient approaches zero. Hence, by plotting the reduced density gradient (*s*) as a function of the density multiplied by the sign of the second eigenvalue of the Hessian matrix sign(λ_2)ρ, which effectively distinguishes if the interaction is attractive [negative] or repulsive [positive]), a series of peaks are obtained, which can be attributed to each NCI and its attractive or repulsive behavior, as described elsewhere.[68,69] Attractive interactions include hydrogen bonding, dipole−dipole, and London dispersion interactions, while very weak interactions correspond to long-range van der Waals interactions; repulsive interactions mainly encompass steric effects.

The NCI analysis of the high coverage model with 4 Cys per unit cell is displayed in Figure 10. According to this representation, the three strongest attractive interactions correspond to the hydrogen bonding between the NH_2 group and COO^- or S^-. Interestingly, these attractive interactions offset the steric clashes between Cys molecules, making this configuration stable with a ΔG_{ads} per Cys of ca. −0.10 eV (Figure 8d). However, the ability of Cys molecules to create such strong attractive interactions is hindered upon the addition of a fifth Cys (high coverage, Figure 8e), which is

DOI: 10.1021/acsnano.9b07513
ACS Nano XXXX, XXX, XXX−XXX

derived in weaker attractive interactions and stronger steric clashes leading to the unfavorable adsorption of further Cys ligands. The NCI plots for both low and high coverage models are presented in Figure S6 in the Supporting Information.

Overall, DFT calculations clearly show that, at low concentrations, Cys molecules are predominantly adsorbed on the Cd^{2+} ions of the QD surface in a tridentate mode via the S^-, NH_2, and COO^- groups. However, this trend in coordination is altered as the Cys concentration increases. Particularly, the high coverage models predict the prevalence of bidentate Cys ligands bound via the S^- and NH_2 groups, with the possibility of ligands present in a monodentate coordination via the S^- moiety. These results are in good agreement with the experimental data observed in the NMR and FTIR spectra at low and high Cys concentrations, showing the same trend in the coordination change with concentration.

CONCLUSIONS

Thus, in this work the influence of chiral Cys ligand concentration on the chiroptical response intensity of CdSe/CdS QDs has been investigated. Experiments demonstrated that QD CD signal intensity increases with Cys concentration at the beginning, then reaches a maximum and decreases at high Cys concentrations. We found that the intensity of CD signal showed a 10-fold increase at an optimal Cys concentration of 0.26 mg/mL. NMR and FTIR analyses demonstrated that Cys molecules adopt different binding configurations on the QD surface at different ligand concentrations. Particularly, at high concentrations, Cys molecules are most likely bound to the QD surface via the S^- and NH_2 groups, whereas at low concentrations, they are coordinated via all three functional groups, i.e., S^-, NH_2 and COO^-. Our results also suggest that tridentate and bidentate configurations of bound Cys are almost diasterioisomeric configurations, which gives rise to opposite CD signals. At high Cys concentrations, however, at which large amounts of Cys are bound in a bidentate mode, the CD signal can decrease as a result of superposition of those opposite CD signals. These results were fully supported by our DFT calculations, which indicate a clear change in the coordination mode of Cys molecules as the ligand concentration increases. Furthermore, simulations indicated that variations in the binding modes are caused by noncovalent interactions between the ligands. Overall, this combined experimental and theoretical work demonstrated that chiroptical properties of QDs are strongly dependent on the concentration and binding modes of chiral ligands, which is very important for the understanding of chiroptical phenomena at the nanoscale and the future design of advanced optically active nanomaterials. Since chirality plays a key role in chemical and biological systems, the results described herein are of considerable interest, from both a fundamental and practical point of view, and may usefully contribute to the development of potential applications of optically active nanocrystals, including optical chiral sensing, detection of various enantiomeric species, enantiospecific separation, asymmetric catalysis, and biological imaging.

MATERIALS AND METHODS

Chemicals. All chemical reagents were of analytical grade and used as purchased without further purification. L-Cys and D-Cys, HPLC acetone, HPLC hexane, HPLC toluene, oleic acid (90%), 1-octadecene (ODE, 90%), selenium (99.99%), sulfur (99.998%), oleylamine (98%), trioctylphosphine (TOP, 97%), and trioctylphosphine oxide (TOPO, 99%) were purchased from Sigma–Aldrich. Cadmium oxide (99.995%) were purchased from Alfa Aesar. Hydrochloric acid, methanol, chloroform, and potassium hydroxide were purchased from Sigma–Aldrich and used for phase-transfer procedure. Toluene and distilled water (Millipore) were used as solvents.

Synthesis of CdSe QDs. CdSe QDs were synthesized following the protocol described in a previous work.[33] A 0.2 M Cd-oleate stock solution (in ODE) was prepared by adding 0.257 g of CdO to 2 mL of oleic acid in 8 mL of ODE, degassing it under reduced pressure, and then heating to 300 °C under argon, followed by cooling to 30 °C. A 1.5 M Se-TOP solution was prepared by dissolving 0.3553 g of Se in 3 mL of TOP, using sonication under argon. Next, CdSe core nanocrystals were prepared by mixing 4.5 g of octadecylamine, 1.5 g of TOPO, 12 g of ODE, and 3 mL of Cd-oleate solution in a three-neck round-bottom flask. This mixture was then degassed at 90 °C for 30 min, flashed with argon, and then heated to 290 °C. Upon reaching this temperature, the Se-TOP solution above was injected and the reaction vessel was immediately removed from the heat. The solution was allowed to cool to room temperature, followed by the addition of 20 mL of acetone to the mixture to isolate CdSe QDs.

Synthesis of CdSe/CdS QDs. This synthesis was also performed as reported in a previous work.[33] The volumes used were calculated using the SILAR approach to control the precise thickness of CdS deposited. Initially, a 0.1 M cadmium stock solution was prepared by adding 0.514 g (4 mmol) of CdO to 8 mL of oleic acid and 32 mL of ODE, which was degassed, then heated to 300 °C under argon, and finally cooled to 30 °C. A 0.1 M sulfur stock solution was prepared by dissolving 0.128 g (4 mmol) of S in 40 mL of ODE at 180 °C under argon (should appear as a yellow solution, changing from a very light straw color at 120 °C). Next, 33.2 mL of oleylamine, 66.4 mL of ODE, and 2.24×10^{-6} mol of QDs were added to a 250-mL three-neck round-bottom flask. This was heated to 50 °C and degassed for 60 min, followed by injection of 5.7 mL of Cd stock solution and, finally, heating to 230 °C. After 10 min at this temperature, 5.7 mL of S solution was injected, followed by a 10 min wait. The reaction mixture was then heated to 250 °C for 1 h to fully allow the reaction to complete the growth of the first shell. At this time, 25 mL of the reaction solution was removed and allowed to cool under argon, producing the first sample. Subsequently, following the same procedure, 6.2 mL of 0.1 M Cd and S stock solution was added to grow the second shell, removing 25 mL of reaction solution again to produce the second shell sample. This overall procedure was repeated three times, injecting 6 mL for shell 3, 5.2 mL for shell 4, and 3.85 mL for shell 5, following which the solution was allowed to cool to room temperature, at which time 20 mL of acetone was added to precipitate the samples using centrifugation. The precipitate was redispersed in a minimum volume of hexane and then precipitated using acetone. This procedure was repeated twice to produce a cleaned QD sample.

Ligand Exchange of the CdSe/CdS Core/Shell Quantum Dots with Chiral Cysteine Molecules. Cysteine ligand exchange was performed using the previously reported method,[14,33] with some modifications. Briefly, 750 μL of CdSe/CdS QDs in chloroform with the concentration of 12 μM was precipitated with methanol (1 mL). Centrifugation was used to separate precipitated QDs from solution, which were redissolved in chloroform (750 μL). Then, 75 μL of a cysteine solution in methanol (0.27 mM) was added to the QD chloroform solution, shaken, and left for 2 min. Next, 750 μL of an aqueous 0.01 M KOH solution was added, therefore adjusting the pH to 13 and forming a bilayer solution. The layers were then mixed by gentle inversions multiple times until the majority of the QDs were transferred to the aqueous layer, as indicated by color change. The sample was then centrifuged in order to fully separate the layers and remove aggregates (15 000 rpm, 1 min). Finally, the aqueous layer was extracted using a pipet and stored between 2 and 5 °C.

Preparation of CdSe/CdS QD Solutions with Cys for NMR Analysis. After ligand exchange, QDs still contained some amount of residual hydrophobic molecules on the surface. In order to remove those molecules, the QDs were purified after phase transfer by washing with excess cysteine (20 mg/mL) using Millipore Sigma

DOI: 10.1021/acsnano.9b07513
ACS Nano XXXX, XXX, XXX–XXX

Amicon Ultra centrifugal filter units. To obtain a sample with a low amount of Cys the excess cysteine was removed by washing of QDs with a pH 13 KOH solution. High Cys concentration solution pH was adjusted to 13 via the addition of concentrated KOH solution. Cys-QD solutions for NMR analysis were prepared and measured under argon atmosphere to avoid Cys oxidation. H_2O was used instead of D_2O to avoid the replacement of H atoms in amino group of Cys with D atoms, which could influence the results of the measurements.

Preparation of CdSe/CdS QD Samples with Cys for FTIR Analysis. After ligand exchange, QDs were washed several times with an excess of Cys (20 mg/mL) to replace all the residual surfactant ligands, which could be the cause of experimental artifacts using Millipore Sigma Amicon Ultra centrifugal filter units. Sample with a high amount of Cys were prepared via the precipitation of QDs with acetone from the solution with a Cys concentration of 20 g/mL. To obtain the sample with the low amount of Cys, the QDs were washed two times with KOH solution with pH 13 to gradually decrease the amount of Cys and then were precipitated with acetone. Samples were dried at a temperature of 70 °C overnight to remove remains of the water and acetone.

Equipment. UV-vis absorption spectroscopy was performed using a Cary 50 spectrophotometer (Varian, Australia). CD spectroscopy was performed using a Jasco J-815 CD spectrometer operating under a N_2 flow of 5−8 L/min. TEM was performed using a FEI Titan electron microscope operating at a beam voltage of 300 kV. FTIR spectra were recorded on a Spectrum 100 instrument (PerkinElmer). NMR studies were performed using a Bruker Avance III 400 NMR spectrometer operating at 400.23 MHz for ^{1}H and 100.64 MHz for ^{13}C. The NMR spectra were acquired and processed using Bruker Tospin 3.6 software. Standard ^{1}H and ^{13}C (proton -decoupled) pulse sequences were taken from the Bruker pulse program library.

Computational Methods. DFT calculations reported in this work were performed using projector-augmented wave (PAW) pseudopotentials[70] and the Perdew−Burke−Ernzerhof (PBE) functional,[71] as implemented in the Vienna *Ab Initio* Simulation Package (VASP) code, version 5.4.4.[72,73] In order to determine the optimal parameters for the optimization of the CdS bulk, the reciprocal space was sampled using Γ-centered *k*-point grids of size 3 × 3 × 3, 5 × 5 × 5, 7 × 7 × 7, and 9 × 9 × 9 and an energy cutoff of 500 eV. Complying an energy convergence criterion of 1 meV/atom, a Γ-centered *k*-point grid of size 5 × 5 × 5 was used for following bulk calculations.

Periodic slab calculations were performed using a plane wave kinetic energy cutoff of 500 eV and a vacuum spacing of 15 Å along the *z*-axis, sampling the reciprocal space using a Γ-centered *k*-point grid of size 3 × 3 × 1, based on the optimized *k*-point density found in the above bulk calculations. To model the surface of the core/shell QD, a four-layer Cd-terminated CdS(0001) surface with a (3 × 3) periodicity was employed for all the Cys adsorption calculations, which is equivalent to the experimentally predominant (0002) plane observed in the XRD patterns of CdS, CdSe, and CdSe/CdS heterostructures.[74] In these structures, atoms in the two topmost layers were allowed to relax from their initial positions, whereas the rest of the atoms were kept fixed at their bulk positions.

To assess the influence of Cys concentration on their binding modes, an initial Cys molecule was adsorbed on the slab with a net charge of −2 per molecule, which accounts for the 2 negative charges from the deprotonated carboxyl and thiol groups in Cys at the experimental pH (pH 13). A total of 16 calculations were performed for the adsorption of 1 Cys molecule on the surface, considering all possible starting binding modes (Figure 3) while sampling all the available surface adsorption sites. To simulate an increase in the surface ligand concentration, the following calculations were performed: (i) a second Cys was adsorbed on the lowest energy structure containing 1 Cys ligand, and (ii) two Cys were adsorbed on the pristine CdS(0001) surface to account for other potential binding modes. This process was repeated with the addition of further Cys molecules, until the computed ΔG_{ads} of an additional ligand became endergonic. This procedure resulted in a total of 67 calculations; the most stable ones are represented in Figure 8.

Gibbs corrections to the DFT-calculated potential energies were computed for the QD surfaces with one adsorbed Cys at the experimental temperature of 300 K and pressure of 1 atm. These corrections included the zero point energy (ZPE), vibrational enthalpy, and entropy terms obtained by means of the harmonic approximation using the Thermochemistry module implemented in the Atomic Simulation Environment (ASE) package.[75] The Gibbs energy for the isolated Cys molecule was calculated at the same temperature and pressure by means of the ideal gas approximation, adding the ZPE and the translational, rotational, vibrational, and electronic contributions of the constant-pressure heat capacity, plus a k_B term. The Gibbs corrections obtained for the lowest energy configurations with a single monodentate, bidentate, and tridentate Cys ligand were employed to calculate the Gibbs corrections for higher coverages. For instance, the Gibbs energy of a high coverage model with 2 monodentate and 2 bidentate ligands was calculated as follows:

$$G_{2\text{mono}+2\text{bi}} = E_{2\text{mono}+2\text{bi}} + 2\Delta G_{\text{mono}} + 2\Delta G_{\text{bi}}$$

where $G_{2\text{mono}+2\text{bi}}$ is the Gibbs energy of a set of two monodentate and two bidentate Cys adsorbed on the surface, $E_{2\text{mono}+2\text{bi}}$ is the potential energy of the same system, and ΔG_{mono} and ΔG_{bi} are the Gibbs energy corrections of adsorbed monodentate and bidentate Cys ligands on their own, in their lowest energy configurations. Gibbs energies of adsorption of Cys molecules on the QD surface were calculated with the following formula:

$$\Delta G_{n\times\text{Cys}^*} = G_{n\times\text{Cys}^*} - n \times G_{\text{cys}} - E_*$$

where $\Delta G^*_{n\times\text{Cys}}$ is the Gibbs energy of adsorption of *n* Cys molecules (the asterisk symbol (*) indicates that the ligands are adsorbed on a surface site), $G^*_{n\times\text{Cys}}$ is the total Gibbs energy of the system, G_{cys} is the Gibbs energy of a Cys molecule in the gas phase, and E^* is the potential energy of the clean surface.

Finally, noncovalent interactions within the ligand phase were calculated by means of the Critic2 software,[76] by computing the electron density, $\rho(r)$, and reduced density gradient, $s(r)$:

$$s(r) = \frac{|\nabla\rho(r)|}{2(3\pi^2)^{1/3}\rho(r)^{4/3}}$$

ASSOCIATED CONTENT

Supporting Information

The Supporting Information is available free of charge on the ACS Publications Web site at DOI: The Supporting Information is available free of charge on the ACS Publications website at DOI: 10.1021/acsnano.9b07513.

CdSe/CdS QD TEM and PL data, D-Cys CdSe/CdS QD CD spectra, full free Cys, Cys-, and oleylamine-capped CdSe/CdS QD FTIR spectra, differential adsorption vs Cys coverage, NCI plots of DFT models. All the DFT data underlying this work, including the Cartesian coordinates of the modeled structures and energies, are available at the following ioChem-BD online dataset: 10.19061/iochem-bd-6-20 (PDF)

AUTHOR INFORMATION

Corresponding Authors

*E-mail: vkuznets@tcd.ie (V. A. Kuznetsova).
*E-mail: garciamm@tcd.ie (M. Garcia-Melchor).
*E-mail: igounko@tcd.ie (Y. K. Gun'ko).

ORCID

Nadezda Prochukhan: 0000-0002-2535-7132
Finn Purcell-Milton: 0000-0002-3591-9477
Anastasia K. Visheratina: 0000-0001-7839-6496
Marina Martinez-Carmona: 0000-0002-2026-6266

DOI: 10.1021/acsnano.9b07513
ACS Nano XXXX, XXX, XXX−XXX

Yulia Gromova: 0000-0001-8826-8543
Max Garcia-Melchor: 0000-0003-1348-4692
Yurii K. Gun'ko: 0000-0002-4772-778X

Author Contributions

The manuscript was written through contributions of all authors. All authors have given approval to the final version of the manuscript.

Author Contributions

[∇]These authors contributed equally.

Notes

The authors declare no competing financial interest.

ACKNOWLEDGMENTS

Authors gratefully thank Trinity College Dublin and SFI Bioeconomy Research Centre, BEACON (No. SFI 16/RC/3889) for financial support. Particularly, E.M.-T. acknowledges funding from the Ussher Postgraduate Scholarships Programme, generously funded through alumni donations and Trinity's Commercial Revenue Unit. The DJEI/DES/SFI/HEA Irish Centre for High-End Computing (ICHEC) is also acknowledged for the generous provision of computational facilities and support. V.A.K. and Y.K.G. acknowledge support from the Federal Target Program for Research and Development of the Ministry of Science and Higher Education of the Russian Federation (No. 14.587.21.0047, identifier RFMEFI58718x0047).

REFERENCES

(1) Milton, F. P.; Govan, J.; Mukhina, M. V.; Gun'ko, Y. K. The Chiral Nano-World: Chiroptically Active Quantum Nanostructures. *Nanoscale Horiz* **2016**, *1*, 14−26.

(2) Ma, W.; Xu, L.; de Moura, A. F.; Wu, X.; Kuang, H.; Xu, C.; Kotov, N. A. Chiral Inorganic Nanostructures. *Chem. Rev.* **2017**, *117*, 8041−8093.

(3) Moloney, M. P.; Gun'ko, Y. K.; Kelly, J. M. Chiral Highly Luminescent CdS Quantum Dots. *Chem. Commun.* **2007**, *38*, 3900−3902.

(4) Ben-Moshe, A.; Maoz, B. M.; Govorov, A. O.; Markovich, G. Chirality and Chiroptical Effects in Inorganic Nanocrystal Systems with Plasmon and Exciton Resonances. *Chem. Soc. Rev.* **2013**, *42*, 7028−7041.

(5) Govan, J.; Gun'ko, Y. K. Recent Progress in Chiral Inorganic Nanostructures. In *Nanoscience*, Vol. 3; O'Brien, P., Thomas, P. J., Eds.; The Royal Society of Chemistry: London, 2016; pp 1−30.

(6) Kumar, J.; Thomas, K. G.; Liz-Marzán, L. M. Nanoscale Chirality in Metal and Semiconductor Nanoparticles. *Chem. Commun.* **2016**, *52*, 12555−12569.

(7) Martynenko, I.; Kuznetsova, V.; Orlova, A.; Kanaev, P.; Gromova, Y.; Maslov, V.; Baranov, A.; Fedorov, A. ZnSe/ZnS Quantum Dots - Photosensitizer Complexes: Optical Properties and Cancer Cell Photodynamic Destruction Effect. *Proc. SPIE* **2014**, 91263C.

(8) Han, C.; Li, H. Chiral Recognition of Amino Acids Based on Cyclodextrin-Capped Quantum Dots. *Small* **2008**, *4*, 1344−1350.

(9) Carrillo-Carrión, C.; Cárdenas, S.; Simonet, B. M.; Valcárcel, M. Selective Quantification of Carnitine Enantiomers Using Chiral Cysteine-Capped CdSe(ZnS) Quantum Dots. *Anal. Chem.* **2009**, *81*, 4730−4733.

(10) Xia, Y.; Zhou, Y.; Tang, Z. Chiral Inorganic Nanoparticles: Origin, Optical Properties and Bioapplications. *Nanoscale* **2011**, *3*, 1374−1382.

(11) Li, Y.; Zhou, Y.; Wang, H.-Y.; Perrett, S.; Zhao, Y.; Tang, Z.; Nie, G. Chirality of Glutathione Surface Coating Affects the Cytotoxicity of Quantum Dots. *Angew. Chem., Int. Ed.* **2011**, *50*, 5860−5864.

(12) Delgado-Pérez, T.; Bouchet, L. M.; de la Guardia, M.; Galian, R. E.; Pérez-Prieto, J. Sensing Chiral Drugs by Using CdSe/ZnS Nanoparticles Capped with N-Acetyl-L-Cysteine Methyl Ester. *Chem. - Eur. J.* **2013**, *19*, 11068−11076.

(13) Ghasemi, F.; Hormozi-Nezhad, M. R.; Mahmoudi, M. Time-Resolved Visual Chiral Discrimination of Cysteine Using Unmodified CdTe Quantum Dots. *Sci. Rep.* **2017**, *7*, 890.

(14) Martynenko, I. V.; Kuznetsova, V. A.; Litvinov, I. K.; Orlova, A. O.; Maslov, V. G.; Fedorov, A. V.; Dubavik, A.; Purcell-Milton, F.; Gun'ko, Y. K.; Baranov, A. V. Enantioselective Cellular Uptake of Chiral Semiconductor Nanocrystals. *Nanotechnology* **2016**, *27*, 075102−075109.

(15) Visheratina, A. K.; Purcell-Milton, F.; Serrano-García, R.; Kuznetsova, V. A.; Orlova, A. O.; Fedorov, A. V.; Baranov, A. V.; Gun'ko, Y. K. Chiral Recognition of Optically Active $CoFe_2O_4$ magnetic Nanoparticles by CdSe/CdS Quantum Dots Stabilised with Chiral Ligands. *J. Mater. Chem. C* **2017**, *5*, 1692−1698.

(16) Kuznetsova, V. A.; Visheratina, A. K.; Ryan, A.; Martynenko, I. V.; Loudon, A.; Maguire, C. M.; Purcell-Milton, F.; Orlova, A. O.; Baranov, A. V.; Fedorov, A. V.; Prina-Mello, A.; Volkov, Y.; Gun'Ko, Y. K. Enantioselective Cytotoxicity of ZnS:Mn Quantum Dots in A549 Cells. *Chirality* **2017**, *29*, 403−408.

(17) Zhu, F.; Li, X.; Li, Y.; Yan, M.; Liu, S. Enantioselective Circular Dichroism Sensing of Cysteine and Glutathione with Gold Nanorods. *Anal. Chem.* **2015**, *87*, 357−361.

(18) Hou, X.; Ke, C.; Bruns, C. J.; McGonigal, P. R.; Pettman, R. B.; Stoddart, J. F. Tunable Solid-State Fluorescent Materials for Supramolecular Encryption. *Nat. Commun.* **2015**, *6*, 6884−6892.

(19) Li, W.-S.; Shen, Y.; Chen, Z.-J.; Cui, Q.; Li, S.-S.; Chen, L.-J. Demonstration of Patterned Polymer-Stabilized Cholesteric Liquid Crystal Textures for Anti-Counterfeiting Two-Dimensional Barcodes. *Appl. Opt.* **2017**, *56*, 601−606.

(20) Zhu, Z.; Guo, J.; Liu, W.; Li, Z.; Han, B.; Zhang, W.; Tang, Z. Controllable Optical Activity of Gold Nanorod and Chiral Quantum Dot Assemblies. *Angew. Chem., Int. Ed.* **2013**, *52*, 13571−13575.

(21) Nguyen, T.-D.; Hamad, W. Y.; MacLachlan, M. J. CdS Quantum Dots Encapsulated in Chiral Nematic Mesoporous Silica: New Iridescent and Luminescent Materials. *Adv. Funct. Mater.* **2014**, *24*, 777−783.

(22) Hu, T.; Isaacoff, B. P.; Bahng, J. H.; Hao, C.; Zhou, Y.; Zhu, J.; Li, X.; Wang, Z.; Liu, S.; Xu, C.; Biteen, J.; Kotov, N. A. Self-Organization of Plasmonic and Excitonic Nanoparticles into Resonant Chiral Supraparticle Assemblies. *Nano Lett.* **2014**, *14*, 6799−6810.

(23) Yeom, J.; Yeom, B.; Chan, H.; Smith, K. W.; Dominguez-Medina, S.; Bahng, J. H.; Zhao, G.; Chang, W.-S.; Chang, S.-J.; Chuvilin, A.; Melnikau, D.; Rogach, A. L.; Zhang, P.; Link, S.; Král, P.; Kotov, N. A. Chiral Templating of Self-Assembling Nanostructures by Circularly Polarized Light. *Nat. Mater.* **2015**, *14*, 66−72.

(24) Naaman, R.; Waldeck, D. H. Spintronics and Chirality: Spin Selectivity in Electron Transport Through Chiral Molecules. *Annu. Rev. Phys. Chem.* **2015**, *66*, 263−281.

(25) Bloom, B. P.; Kiran, V.; Varade, V.; Naaman, R.; Waldeck, D. H. Spin Selective Charge Transport through Cysteine Capped CdSe Quantum Dots. *Nano Lett.* **2016**, *16*, 4583−4589.

(26) Bloom, B. P.; Graff, B. M.; Ghosh, S.; Beratan, D. N.; Waldeck, D. H. Chirality Control of Electron Transfer in Quantum Dot Assemblies. *J. Am. Chem. Soc.* **2017**, *139*, 9038−9043.

(27) Varga, K.; Tannir, S.; Haynie, B. E.; Leonard, B. M.; Dzyuba, S. V.; Kubelka, J.; Balaz, M. CdSe Quantum Dots Functionalized with Chiral, Thiol-Free Carboxylic Acids: Unraveling Structural Requirements for Ligand-Induced Chirality. *ACS Nano* **2017**, *11*, 9846−9853.

(28) Choi, J. K.; Haynie, B. E.; Tohgha, U.; Pap, L.; Elliott, K. W.; Leonard, B. M.; Dzyuba, S. V.; Varga, K.; Kubelka, J.; Balaz, M. Chirality Inversion of CdSe and CdS Quantum Dots without Changing the Stereochemistry of the Capping Ligand. *ACS Nano* **2016**, *10*, 3809−3815.

(29) Tohgha, U.; Deol, K. K.; Porter, A. G.; Bartko, S. G.; Choi, J. K.; Leonard, B. M.; Varga, K.; Kubelka, J.; Muller, G.; Balaz, M. Ligand Induced Circular Dichroism and Circularly Polarized

DOI: 10.1021/acsnano.9b07513
ACS Nano XXXX, XXX, XXX−XXX

Luminescence in CdSe Quantum Dots. *ACS Nano* **2013**, *7*, 11094−11102.
(30) Tohgha, U.; Varga, K.; Balaz, M. Achiral CdSe Quantum Dots Exhibit Optical Activity in the Visible Region upon Post-Synthetic Ligand Exchange with d- or l-Cysteine. *Chem. Commun.* **2013**, *49*, 1844−1846.
(31) Cheng, J.; Hao, J.; Liu, H.; Li, J.; Li, J.; Zhu, X.; Lin, X.; Wang, K.; He, T. Optically Active CdSe-Dot/CdS-Rod Nanocrystals with Induced Chirality and Circularly Polarized Luminescence. *ACS Nano* **2018**, *12*, 5341−5350.
(32) Puri, M.; Ferry, V. E. Circular Dichroism of CdSe Nanocrystals Bound by Chiral Carboxylic Acids. *ACS Nano* **2017**, *11*, 12240−12246.
(33) Purcell-Milton, F.; Visheratina, A. K.; Kuznetsova, V. A.; Ryan, A.; Orlova, A. O.; Gun'ko, Y. K. Impact of Shell Thickness on Photoluminescence and Optical Activity in Chiral CdSe/CdS Core/Shell Quantum Dots. *ACS Nano* **2017**, *11*, 9207−9214.
(34) Martynenko, I. V.; Baimuratov, A. S.; Osipova, V. A.; Kuznetsova, V. A.; Purcell-Milton, F.; Rukhlenko, I. D.; Fedorov, A. V.; Gun'Ko, Y. K.; Resch-Genger, U.; Baranov, A. V. Excitation Energy Dependence of the Photoluminescence Quantum Yield of Core/Shell CdSe/CdS Quantum Dots and Correlation with Circular Dichroism. *Chem. Mater.* **2018**, *30*, 465−471.
(35) Moloney, M. P.; Govan, J.; Loudon, A.; Mukhina, M.; Gun'ko, Y. K. Preparation of Chiral Quantum Dots. *Nat. Protoc.* **2015**, *10*, 558−573.
(36) Mukhina, M. V.; Maslov, V. G.; Baranov, A. V.; Fedorov, A. V.; Orlova, A. O.; Purcell-Milton, F.; Govan, J.; Gun'ko, Y. K. Intrinsic Chirality of CdSe/ZnS Quantum Dots and Quantum Rods. *Nano Lett.* **2015**, *15*, 2844−2851.
(37) Mukhina, M. V.; Maslov, V. G.; Korsakov, I. V.; Purcell Milton, F.; Loudon, A.; Baranov, A. V.; Fedorov, A. V.; Gun'ko, Y. K. Optically Active II-VI Semiconductor Nanocrystals *via* Chiral Phase Transfer. *MRS Proc.* **2015**, *1793*, 27−33.
(38) Ben Moshe, A.; Szwarcman, D.; Markovich, G. Size Dependence of Chiroptical Activity in Colloidal Quantum Dots. *ACS Nano* **2011**, *5*, 9034−9043.
(39) Ben Moshe, A.; Markovich, G.; Tang, Z. Optically Active and Chiral Semiconductor Nanocrystals. In *Chiral Nanomaterials: Preparation, Properties and Applications*; Tang, Z., Ed.; Wiley−VCH: Weinheim, Germany; 2017; pp 85−98.
(40) Ben-Moshe, A.; Teitelboim, A.; Oron, D.; Markovich, G. Probing the Interaction of Quantum Dots with Chiral Capping Molecules Using Circular Dichroism Spectroscopy. *Nano Lett.* **2016**, *16*, 7467−7473.
(41) Elliott, S. D.; Moloney, M. P.; Gun'ko, Y. K. Chiral Shells and Achiral Cores in CdS Quantum Dots. *Nano Lett.* **2008**, *8*, 2452−2457.
(42) Zhou, Y.; Yang, M.; Sun, K.; Tang, Z.; Kotov, N. A. Similar Topological Origin of Chiral Centers in Organic and Nanoscale Inorganic Structures: Effect of Stabilizer Chirality on Optical Isomerism and Growth of CdTe Nanocrystals. *J. Am. Chem. Soc.* **2010**, *132*, 6006−6013.
(43) Zhou, Y.; Zhu, Z.; Huang, W.; Liu, W.; Wu, S.; Liu, X.; Gao, Y.; Zhang, W.; Tang, Z. Optical Coupling Between Chiral Biomolecules and Semiconductor Nanoparticles: Size-Dependent Circular Dichroism Absorption. *Angew. Chem., Int. Ed.* **2011**, *50*, 11456−11459.
(44) Govorov, A. O.; Fan, Z.; Hernandez, P.; Slocik, J. M.; Naik, R. R. Theory of Circular Dichroism of Nanomaterials Comprising Chiral Molecules and Nanocrystals: Plasmon Enhancement, Dipole Interactions, and Dielectric Effects. *Nano Lett.* **2010**, *10*, 1374−1382.
(45) Tsay, J. M.; Doose, S.; Pinaud, F.; Weiss, S. Enhancing the Photoluminescence of Peptide-Coated Nanocrystals with Shell Composition and UV Irradiation. *J. Phys. Chem. B* **2005**, *109*, 1669−1674.
(46) Harris, R. D.; Amin, V. A.; Lau, B.; Weiss, E. A. Role of Interligand Coupling in Determining the Interfacial Electronic Structure of Colloidal CdS Quantum Dots. *ACS Nano* **2016**, *10*, 1395−1403.
(47) Visheratina, A. K.; Orlova, A. O.; Purcell-Milton, F.; Kuznetsova, V. A.; Visheratin, A. A.; Kundelev, E. V.; Maslov, V. G.; Baranov, A. V.; Fedorov, A. V.; Gun'Ko, Y. K. Influence of CdSe and CdSe/CdS Nanocrystals on the Optical Activity of Chiral Organic Molecules. *J. Mater. Chem. C* **2018**, *6*, 1759−1766.
(48) Mukhina, M. V.; Maslov, V. G.; Baranov, A. V.; Artemyev, M. V.; Orlova, A. O.; Fedorov, A. V. Anisotropy of Optical Transitions in Ordered Ensemble of CdSe Quantum Rods. *Opt. Lett.* **2013**, *38*, 3426−3428.
(49) Gao, X.; Zhang, X.; Deng, K.; Han, B.; Zhao, L.; Wu, M.; Shi, L.; Lv, J.; Tang, Z. Excitonic Circular Dichroism of Chiral Quantum Rods. *J. Am. Chem. Soc.* **2017**, *139*, 8734−8739.
(50) Govan, J. E.; Jan, E.; Querejeta, A.; Kotov, N. A.; Gun'ko, Y. K. Chiral Luminescent CdS Nano-Tetrapods. *Chem. Commun.* **2010**, *46*, 6072−6074.
(51) Frederick, M. T.; Amin, V. A.; Swenson, N. K.; Ho, A. Y.; Weiss, E. A. Control of Exciton Confinement in Quantum Dot−Organic Complexes through Energetic Alignment of Interfacial Orbitals. *Nano Lett.* **2013**, *13*, 287−292.
(52) Li, T.; Park, H. G.; Lee, H.-S.; Choi, S.-H. Circular Dichroism Study of Chiral Biomolecules Conjugated with Silver Nanoparticles. *Nanotechnology* **2004**, *15*, S660−S663.
(53) Mahler, B.; Spinicelli, P.; Buil, S.; Quelin, X.; Hermier, J.-P.; Dubertret, B. Towards Non-Blinking Colloidal Quantum Dots. *Nat. Mater.* **2008**, *7*, 659.
(54) Gautier, C.; Bürgi, T. Chiral Inversion of Gold Nanoparticles. *J. Am. Chem. Soc.* **2008**, *130*, 7077−7084.
(55) Kuno, J.; Imamura, Y.; Katouda, M.; Tashiro, M.; Kawai, T.; Nakashima, T. Inversion of Optical Activity in the Synthesis of Mercury Sulfide Nanoparticles: Role of Ligand Coordination. *Angew. Chem., Int. Ed.* **2018**, *57*, 12022−12026.
(56) Kurihara, T.; Matano, A.; Noda, Y.; Takegoshi, K. Rotational Motion of Ligand-Cysteine on CdSe Magic-Sized Clusters. *J. Phys. Chem. C* **2019**, *123*, 14993−14998.
(57) Kurihara, T.; Noda, Y.; Takegoshi, K. Capping Structure of Ligand−Cysteine on CdSe Magic-Sized Clusters. *ACS Omega* **2019**, *4*, 3476−3483.
(58) Kurihara, T.; Noda, Y.; Takegoshi, K. Quantitative Solid-State NMR Study on Ligand−Surface Interaction in Cysteine-Capped CdSe Magic-Sized Clusters. *J. Phys. Chem. Lett.* **2017**, *8*, 2555−2559.
(59) Cui, Y.; Lou, Z.; Wang, X.; Yu, S.; Yang, M. A Study of Optical Absorption of Cysteine-Capped CdSe Nanoclusters Using First-Principles Calculations. *Phys. Chem. Chem. Phys.* **2015**, *17*, 9222−9230.
(60) Mukhina, M. V.; Korsakov, I. V.; Maslov, V. G.; Purcell-Milton, F.; Govan, J.; Baranov, A. V.; Fedorov, A. V.; Gun'ko, Y. K. Molecular Recognition of Biomolecules by Chiral CdSe Quantum Dots. *Sci. Rep.* **2016**, *6*, 24177.
(61) Kane-Maguire, L. A. P.; Riley, P. J. High Field NMR Study of the Binding of Lead(II) to Cysteine and Glutathione. *J. Coord. Chem.* **1993**, *28*, 105−120.
(62) Drauz, K.; Grayson, I.; Kleemann, A.; Krimmer, H.-P.; Leuchtenberger, W.; Weckbecker, C. Amino Acids. In *Ullmann's Encyclopedia of Industrial Chemistry*; Wiley−VCH Verlag GmbH & Co. KGaA, 2007.
(63) Friedman, J. I.; McMahon, M. T.; Stivers, J. T.; Van Zijl, P. C. M. Indirect Detection of Labile Solute Proton Spectra *via* the Water Signal Using Frequency-Labeled Exchange (FLEX) Transfer. *J. Am. Chem. Soc.* **2010**, *132*, 1813−1815.
(64) Zong, X.; Wang, P.; Kim, S.-G.; Jin, T. Sensitivity and Source of Amine-Proton Exchange and Amide-Proton Transfer Magnetic Resonance Imaging in Cerebral Ischemia. *Magn. Reson. Med.* **2014**, *71*, 118−132.
(65) Cistola, D.; M Small, D.; Hamilton, J. Ionization Behavior of Aqueous Short-Chain Carboxylic Acids: A Carbon-^{13}NMR Study. *J. Lipid Res.* **1982**, *23*, 795−799.
(66) Abraham, A.; Mihaliuk, E.; Kumar, B.; Legleiter, J.; Gullion, T. Solid-State NMR Study of Cysteine on Gold Nanoparticles. *J. Phys. Chem. C* **2010**, *114*, 18109−18114.

DOI: 10.1021/acsnano.9b07513
ACS Nano XXXX, XXX, XXX−XXX

(67) Akbarzadeh, M.; Moosavi-Movahedi, Z.; Shockravi, A.; Jafari, R.; Nazari, K.; Sheibani, N.; Moosavi-Movahedi, A. A. Metallo-Vesicular Catalysis: A Mixture of Vesicular Cysteine/Iron Mediates Oxidative pH Switchable Catalysis. *J. Mol. Catal. A: Chem.* **2016**, *424*, 181−193.
(68) Contreras-García, J.; Boto, R.; Izquierdo-Ruiz, F.; Reva, I.; Woller, T.; Alonso, M. A Benchmark for the Non-Covalent Interaction (NCI) Index Or ... Is It Really All in the Geometry? *Theor. Chem. Acc.* **2016**, *135*, DOI: 10.1007/s00214-016-1977-7.
(69) Johnson, E. R.; Keinan, S.; Mori-Sánchez, P.; Contreras-García, J.; Cohen, A. J.; Yang, W. Revealing Noncovalent Interactions. *J. Am. Chem. Soc.* **2010**, *132*, 6498−6506.
(70) Blöchl, P. E. Projector Augmented-Wave Method. *Phys. Rev. B: Condens. Matter Mater. Phys.* **1994**, *50*, 17953−17979.
(71) Perdew, J. P.; Burke, K.; Ernzerhof, M. Generalized Gradient Approximation Made Simple. *Phys. Rev. Lett.* **1996**, *77*, 3865−3868.
(72) Kresse, G.; Furthmüller, J. Efficiency of *Ab Initio* Total Energy Calculations for Metals and Semiconductors Using a Plane-Wave Basis Set. *Comput. Mater. Sci.* **1996**, *6*, 15−50.
(73) Kresse, G.; Furthmüller, J. Efficient Iterative Schemes for *Ab Initio* Total-Energy Calculations Using a Plane-Wave Basis Set. *Phys. Rev. B: Condens. Matter Mater. Phys.* **1996**, *54*, 11169−11186.
(74) Chauhan, H.; Kumar, Y.; Deka, S. New Synthesis of Two-Dimensional CdSe/CdS Core@shell Dot-in-Hexagonal Platelet Nanoheterostructures with Interesting Optical Properties. *Nanoscale* **2014**, *6*, 10347−10354.
(75) Hjorth Larsen, A.; Jørgen Mortensen, J.; Blomqvist, J.; Castelli, I. E.; Christensen, R.; Dułak, M.; Friis, J.; Groves, M. N.; Hammer, B.; Hargus, C.; Hermes, E. D.; Jennings, P. C.; Bjerre Jensen, P.; Kermode, J.; Kitchin, J. R.; Leonhard Kolsbjerg, E.; Kubal, J.; Kaasbjerg, K.; Lysgaard, S.; Bergmann Maronsson, J.; et al. The Atomic Simulation Environment—a Python Library for Working with Atoms. *J. Phys.: Condens. Matter* **2017**, *29*, 273002−273033.
(76) Otero-de-la-Roza, A.; Johnson, E. R.; Luaña, V. Critic2: A Program for Real-Space Analysis of Quantum Chemical Interactions in Solids. *Comput. Phys. Commun.* **2014**, *185*, 1007−1018.

DOI: 10.1021/acsnano.9b07513
ACS Nano XXXX, XXX, XXX−XXX